Double-scatter cross sections for two-dimensional random rough surfaces that exhibit backscatter enhancement

Ezekiel Bahar

Department of Electrical Engineering, Center for Electro-Optics, University of Nebraska-Lincoln, Lincoln, Nebraska 68588-0511

Magda El-Shenawee

Center for Subsurface Sensing and Imaging Systems, Northeastern University, Boston, Massachusetts 02115-5000

Received May 9, 2000; revised manuscript received July 14, 2000; accepted July 19, 2000

Full-wave solutions are given for the single- and double-scatter radar cross sections for two-dimensional random rough surfaces. High-frequency approximations are used for the double-scatter cross sections in order to express them as numerically tractable four-dimensional integrals. The major contributions to the double-scatter cross sections are associated with the quasi-parallel and quasi-antiparallel double-scatter paths. They come from the neighborhoods of specular points. The enhancement of the backscatter cross sections, which is associated with the quasi-antiparallel double-scatter paths, is observed for both the like- and cross-polarized cross sections. © 2001 Optical Society of America

OCIS codes: 000.3860, 240.0240, 260.0260, 280.0280, 290.4210, 290.5880.

1. INTRODUCTION

In this work, full-wave solutions for the single- and double-scatter radar cross sections for two-dimensional random rough surfaces are given. The solutions are expressed as multidimensional integrals. The high-frequency, physical optics approximations are used to reduce 12-dimensional integral expressions for the double-scatter cross sections, and the large-radius-of-curvature approximation is used. The associated single-scatter cross sections are expressed in closed form. The incident waves are assumed to be plane waves.

Similar to the case for scattering from one-dimensional random rough surfaces,[1] the major contributions to the double-scatter cross sections are associated with two different pairs of propagation paths. They are the quasi-parallel double-scatter paths and the quasi-antiparallel double-scatter paths. The total incoherent double-scatter cross section is the sum of the incoherent quasi-parallel and quasi-antiparallel double-scatter cross sections.

In the high-frequency limit, the major contributions to the single- and double-scatter cross sections come from the neighborhoods of the specular points on the rough surface. Thus, upon integration with respect to the random-rough-surface slopes, the surface element scattering coefficients are evaluated at the specular points. The probability density functions for the slopes and the heights are assumed to be Gaussian. Shadow functions are included in the analysis. Physical interpretations of the analytical results are provided here.

The effects of changing the rough-surface parameters [such as mean square height and mean square slope (mss)] on the double-scatter cross sections are studied. The level and the width of the enhancement in the backscatter direction depend on the mean square height and slope of the rough surface. The sharp backscatter enhancement, which is observed for both the like- and cross-polarized cross sections and for both normal and oblique incident angles, is associated with the quasi-antiparallel double-scatter paths. The medium below the rough interface is characterized by a complex dielectric coefficient. This work is an extension of earlier work that is restricted to scattering in the incident plane by one-dimensional rough surfaces.[1] Thus depolarization is not considered in the earlier work. It is relevant to work in remote sensing and to the design of targets with unusually large backscatter cross sections, such as traffic signs and decoys (reversed stealth).

2. FORMULATION OF THE PROBLEM

The full-wave solutions for the double-scatter electromagnetic far fields $G_d^f(\bar{r})$ from two-dimensional rough surfaces [$y = h(x_s, z_s)$] are given by[1]

$$G_d^f(\bar{r}) = \left(\frac{k_0}{2\pi j}\right)^3 \frac{\exp(-jk_0 r)}{r} \int \frac{D_{2'}(\hat{\mathbf{n}}^f, \hat{\mathbf{n}}')}{n_y^f - n_y'} \times \exp(jk_0 \hat{\mathbf{n}}^f \cdot \mathbf{r}_{s2'}) \times \exp[-jk_0 \hat{\mathbf{n}}' \cdot (\mathbf{r}_{s2'} - \mathbf{r}_{s1'})] \frac{D_{1'}(\hat{\mathbf{n}}', \hat{\mathbf{n}}^i)}{-n_y^i + n_y'} \times \exp(-jk_0 \hat{\mathbf{n}}^i \cdot \mathbf{r}_{s1'}) \frac{\mathrm{d}n_y' \mathrm{d}n_z'}{(1 - n_y'^2 - n_z'^2)^{1/2}} \times U(\mathbf{r}_{s1'}) U(\mathbf{r}_{s2'}) \mathrm{d}x_{s1'} \mathrm{d}z_{s1'} \mathrm{d}x_{s2'} \mathrm{d}z_{s2'} G^i(0), \quad (1)$$

0740-3232/2001/010108-09$15.00

in which the time-harmonic excitations $\exp(j\omega t)$ are assumed and the free-space wave number is $k_0 = \omega\sqrt{\epsilon_0\mu_0}$. The integration in Eq. (1) is over the radar footprint $A = 4l_x l_z$ and components of $\hat{\mathbf{n}}'$. The incident waves are in the direction of the unit vector $\hat{\mathbf{n}}^i$, and the scattered waves are in the direction of the unit vector $\hat{\mathbf{n}}^f$ from the rough surface to the receiver at $\mathbf{r}$. Thus, in terms of the Cartesian unit vectors $\hat{\mathbf{e}}_i$ $(i = x, y, z)$,

$$\hat{\mathbf{n}}^i = n_x^i\hat{\mathbf{e}}_x + n_y^i\hat{\mathbf{e}}_y + n_z^i\hat{\mathbf{e}}_z, \tag{2a}$$

$$\hat{\mathbf{n}}^f = n_x^f\hat{\mathbf{e}}_x + n_y^f\hat{\mathbf{e}}_y + n_z^f\hat{\mathbf{e}}_z, \tag{2b}$$

$$\mathbf{r} = x\hat{\mathbf{e}}_x + y\hat{\mathbf{e}}_y + z\hat{\mathbf{e}}_z, \tag{2c}$$

$$\hat{\mathbf{n}}' = n_x'\hat{\mathbf{e}}_x + n_y'\hat{\mathbf{e}}_y + n_z'\hat{\mathbf{e}}_z. \tag{2d}$$

The scattering matrices at points $1'$ and $2'$ on the rough surface are $D_{1'}(\hat{\mathbf{n}}', \hat{\mathbf{n}}^i)$ and $D_{2'}(\hat{\mathbf{n}}^f, \hat{\mathbf{n}}')$ [see Fig. 1(a)]. The elements of the scattering matrices depend on the local slope of the rough surface.[1,2] Moreover, they depend on the polarization of the incident and scattered waves and the media on both sides of the rough interface. The incident fields are assumed to be plane waves, and the receiver is located in the far field. The wave vectors of the scattered waves from the point $1'$ on the surface are in the direction of the unit vector $\hat{\mathbf{n}}'$ [see Fig. 1(a)]. The position vectors to points $1'$ and $2'$ on the rough surface are given by

$$\mathbf{r}_{s1'} = x_{s1'}\hat{\mathbf{e}}_x + h(x_{s1'}, z_{s1'})\hat{\mathbf{e}}_y + z_{s1'}\hat{\mathbf{e}}_z, \tag{3a}$$

$$\mathbf{r}_{s2'} = x_{s2'}\hat{\mathbf{e}}_x + h(x_{s2'}, z_{s2'})\hat{\mathbf{e}}_y + z_{s2'}\hat{\mathbf{e}}_z. \tag{3b}$$

At high frequencies, the shadow function $U(\mathbf{r}_{s1'})$ is equal to unity if point $1'$ is illuminated by the incident plane wave and visible at point $2'$, and it is zero otherwise; and $U(\mathbf{r}_{s2'})$ is equal to unity if point $2'$ is illuminated by a point source at $1'$ and visible from the receiver,[3] and it is zero otherwise. The double-scatter cross section is obtained on multiplying Eq. (1) by its complex conjugate [see Fig. 1(b)]. The radar cross section for the two-dimensional rough surface is defined as

$$\sigma_T = \frac{4\pi r^2}{A}\left|\frac{G^f}{G^i}\right|^2, \tag{4}$$

$$\begin{aligned}\sigma_T = {} & \frac{k_0^6}{16A\pi^5} \\ & \times \int \frac{D_{2'}(\hat{\mathbf{n}}^f, \hat{\mathbf{n}}')D_{1'}(\hat{\mathbf{n}}', \hat{\mathbf{n}}^i)D_{2''}^*(\hat{\mathbf{n}}^f, \hat{\mathbf{n}}'')D_{1''}^*(\hat{\mathbf{n}}'', \hat{\mathbf{n}}^i)}{(n_y^f - n_y')(n_y^f - n_y'')(-n_y^i + n_y')(-n_y^i + n_y'')} \\ & \times U(\mathbf{r}_{s1'})U(\mathbf{r}_{s1''})U(\mathbf{r}_{s2'})U(\mathbf{r}_{s2''}) \\ & \times \exp\{jk_0[n_x^f(x_{s2'} - x_{s2''}) + n_y^f(h_{2'} - h_{2''}) \\ & + n_z^f(z_{s2'} - z_{s2''})]\}\exp\{-jk_0[n_x'(x_{s2'} - x_{s1'}) \\ & + n_y'(h_{2'} - h_{1'}) + n_z'(z_{s2'} - z_{s1'})]\} \\ & \times \exp\{jk_0[n_x''(x_{s2''} - x_{s1''}) + n_y''(h_{2''} - h_{1''}) \\ & + n_z''(z_{s2''} - z_{s1''})]\}\exp\{-jk_0[n_x^i(x_{s1'} - x_{s1''}) \\ & + n_y^i(h_{1'} - h_{1''}) + n_z^i(z_{s1'} - z_{s1''})]\} \\ & \times \frac{\mathrm{d}n_y'\mathrm{d}n_z'}{(1 - n_y'^2 - n_z'^2)^{1/2}}\frac{\mathrm{d}n_y''\mathrm{d}n_z''}{(1 - n_y''^2 - n_z''^2)^{1/2}} \\ & \times \mathrm{d}x_{s1'}\mathrm{d}z_{s1'}\mathrm{d}x_{s2'}\mathrm{d}z_{s2'}\mathrm{d}x_{s1''}\mathrm{d}z_{s1''}\mathrm{d}x_{s2''}\mathrm{d}z_{s2''}. \end{aligned} \tag{5}$$

In Eq. (5) the superscript $*$ denotes the complex conjugate. For the quasi-parallel double-scatter paths, between points $1'$ and $2'$ and points $1''$ and $2''$ [see Fig. 1(c)] $(n_\alpha', n_\alpha'' < 0$ and $n_\alpha', n_\alpha'' > 0;\ \alpha = x, z)$, the following transformations of variables are used:

$$x_{d1} = x_{s1'} - x_{s1''}, \qquad x_{d2} = x_{s2'} - x_{s2''}, \tag{6a}$$

$$z_{d1} = z_{s1'} - z_{s1''}, \qquad z_{d2} = z_{s2'} - z_{s2''}, \tag{6b}$$

$$x_{a1} = (x_{s1'} + x_{s1''})/2, \qquad x_{a2} = (x_{s2'} + x_{s2''})/2g, \tag{7a}$$

$$z_{a1} = (z_{s1'} + z_{s1''})/2, \qquad z_{a2} = (z_{s2'} + z_{s2''})/2. \tag{7b}$$

Thus, from Eqs. (5)–(7), one gets the following for the quasi-parallel case:

$$\begin{aligned}\sigma_T = {} & \frac{k_0^6}{16A\pi^5} \\ & \times \int \frac{D_{2'}(\hat{\mathbf{n}}^f, \hat{\mathbf{n}}')D_{2'}(\hat{\mathbf{n}}', \hat{\mathbf{n}}^i)D_{2''}^*(\hat{\mathbf{n}}^f, \hat{\mathbf{n}}'')D_{1''}^*(\hat{\mathbf{n}}'', \hat{\mathbf{n}}^i)}{(n_y^f - n_y')(n_y^f - n_y'')(-n_y^i + n_y')(-n_y^i + n_y'')} \\ & \times U(\mathbf{r}_{a1})U(\mathbf{r}_{a2})\exp\{jk_0[n_x^f x_{d2} \\ & - n_x'(0.5x_{d2} - 0.5x_{d1} + x_{a2} - x_{a1}) \\ & + n_x''(-0.5x_{d2} + 0.5x_{d1} + x_{a2} - x_{a1}) - n_x^i x_{d1}]\} \\ & \times \exp\{jk_0[n_z^f z_{d2} - n_z'(0.5z_{d2} - 0.5z_{d1} \\ & + z_{a2} - z_{a1}) + n_z''(-0.5z_{d2} + 0.5z_{d1} + z_{a2} - z_{a1}) \\ & - n_z^i z_{d1}]\}\exp\{jk_0[n_y^f(h_{2'} - h_{2''}) \\ & - n_y'(h_{2'} - h_{1'}) + n_y''(h_{2''} - h_{1''}) - n_y^i(h_{1'} - h_{1''})]\} \\ & \times \frac{\mathrm{d}n_y'\mathrm{d}n_z'}{(1 - n_y'^2 - n_z'^2)^{1/2}}\frac{\mathrm{d}n_y''\mathrm{d}n_z''}{(1 - n_y''^2 - n_z''^2)^{1/2}} \\ & \times \mathrm{d}x_{d1}\mathrm{d}z_{d1}\mathrm{d}x_{d2}\mathrm{d}z_{d2}\mathrm{d}x_{a1}\mathrm{d}z_{a1}\mathrm{d}x_{a2}\mathrm{d}z_{a2}. \end{aligned} \tag{8}$$

For the quasi-parallel case [see Fig. 1(c)], the integrand in Eq. (8) becomes stationary as the points $1'$ and $1''$ as

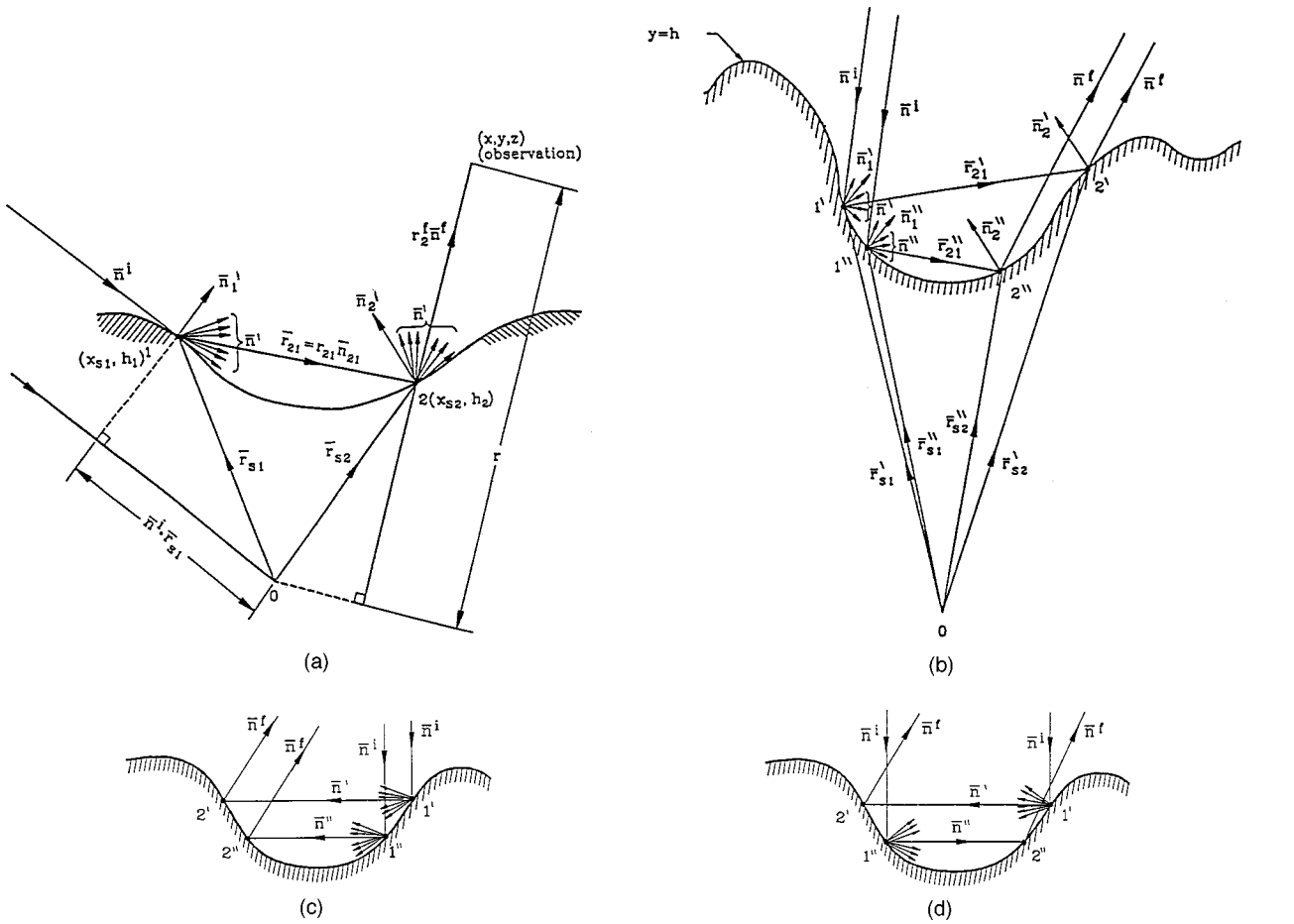

Fig. 1. (a) Double-scatter electromagnetic wave, (b) double-scatter intensity for two-dimensional random rough surfaces, (c) double-scatter quasi-parallel case, (d) double-scatter quasi-antiparallel case.

well as $2'$ and $2''$ approach each other. Thus, to simplify the 12-dimensional integral (8), we use the Taylor-series expansion for the heights at the pair of points $1'$, $1''$ and $2'$, $2''$ in terms of the heights and their derivatives at the midpoints (x_{a1}, z_{a1}) and (x_{a2}, z_{a2}). Upon using Eqs. (6) and (7), we introduce the following approximations in Eq. (8):

$$h_{1'} = h_{a1} + (x_{d1}h_{xa1} + z_{d1}h_{za1})/2, \tag{9a}$$

in which

$$h_{a1} = h_y(x_{a1}, z_{d1}), \qquad h_{xa1} = \partial h/\partial x,$$

$$h_{za1} = \partial h/\partial z \text{ at } x = x_{a1} \text{ and } z = z_{a1}, \tag{9b}$$

$$h_{1''} = h_{a1} - (x_{d1}h_{xa1} + z_{d1}h_{xa1})/2; \tag{9c}$$

thus

$$h_{1'} - h_{1''} = x_{d1}h_{xa1} + z_{d1}h_{xa1}. \tag{9d}$$

Similar expressions are introduced in Eq. (8) for $h_{2'}$ and $h_{2''}$. The integration with respect to $x_{d1}x_{a1}$ is over the diamond-shaped area with corners at $(x_{d1} = 0,\ x_{a1} = l_x)$, $(x_{d1} = 2l_x,\ x_{a1} = 0)$, $(x_{d1} = 0,\ x_{a1} = -l_x)$, and $(x_{d1} = -2l_x,\ x_{a1} = 0)$. Similarly, diamond-shaped areas represent the limits of integration for $x_{d2}x_{a2}$, $z_{d1}z_{a1}$, and $z_{d2}z_{a2}$. Since $k_0 l_x \gg k_0 l_a \gg 1$ and $k_0 l_z \gg k_0 l_c \gg 1$ (l_c is the correlation length for the rough surface), the limits of integration for the variables x_{d1}, x_{d2}, z_{d1}, and z_{d2} in Eq. (1) are assumed to be infinite.

The integral representation of the Dirac delta function is

$$\delta(h_x - h_{xs}) = \frac{1}{2\pi}\int_{-\infty}^{\infty} \exp[ix_d(h_x - h_{xs})]\mathrm{d}x_d. \tag{10}$$

On integration with respect to x_{d1}, x_{d2}, z_{d1}, and z_{d2}, the 12-dimensional integral in Eq. (8) reduces to an eight-dimensional integral containing the following product of four Dirac delta functions:

$$\delta(h_{xa1} - h_{xa1s})\delta(h_{xa2} - h_{xa2s})\delta(h_{za1} - h_{za1s}) \times \delta(h_{za2} - h_{za2s}) \equiv \delta(\nabla h_{a1} - \nabla h_{a1s})\delta(\nabla h_{a2} - \nabla h_{a2s}), \tag{11}$$

in which ∇ is the symbol for gradient and the slopes at the specular points (x_{a1s}, z_{a1s}), and (x_{a2s}, z_{a2s}) are given by

$$h_{xa1s} = -\left(-n_x^i + \frac{n_x' + n_x''}{2}\right) \Big/ \left(-n_y^i + \frac{n_y' + n_y''}{2}\right), \tag{12a}$$

$$h_{xa2s} = -\left(-n_x^f + \frac{n_x' + n_x''}{2}\right) \Big/ \left(-n_y^f + \frac{n_y' + n_y''}{2}\right), \tag{12b}$$

$$h_{za1s} = -\left(-n_z^i + \frac{n_z' + n_z''}{2}\right) \Big/ \left(-n_y^i + \frac{n_y' + n_y''}{2}\right), \tag{12c}$$

$$h_{za2s} = -\left(-n_z^f + \frac{n_z' + n_z''}{2}\right) \Big/ \left(-n_y^f + \frac{n_y' + n_y''}{2}\right). \tag{12d}$$

Thus, in the high-frequency (physical optics) limit, the major contributions to the double-scatter cross sections come from the neighborhoods of the specular points. Equation (8) reduces to

$$\sigma_T^{PQ} = \frac{k_0^2}{\pi A} \sum_{R,S=V,H} \int \frac{D_{2'}^{PS}(\hat{\mathbf{n}}^f, \hat{\mathbf{n}}') D_{1'}^{SQ}(\hat{\mathbf{n}}', \hat{\mathbf{n}}^i) D_{2''}^{*PR}(\hat{\mathbf{n}}^f, \hat{\mathbf{n}}'') D_{1''}^{*RQ}(\hat{\mathbf{n}}'', \hat{\mathbf{n}}')}{(n_y^f - n_y')(n_y^f - n_y'')(n_y^i - n_y')(n_y^i - n_y'')} U(\mathbf{r}_{a1}) U(\mathbf{r}_{a2}) \delta(\nabla h_{a1} - \nabla h_{a1s})$$
$$\times \delta(\nabla h_{a2} - \nabla h_{a2s}) \exp[jk_0(\mathbf{r}_{a1} - \mathbf{r}_{a2}) \cdot (\hat{\mathbf{n}}' - \hat{\mathbf{n}}'')] \frac{\mathrm{d}n_y' \mathrm{d}n_z' \mathrm{d}n_y'' \mathrm{d}n_z'' \mathrm{d}x_{a1} \mathrm{d}x_{a2} \mathrm{d}z_{a1} \mathrm{d}z_{a2}}{n_x' n_x'' [n_y^f - (n_y' + n_y'')/2]^2 [n_y^i - (n_y' + n_y'')/2]^2}, \tag{13}$$

where $\mathbf{r}_{a1}$ and $\mathbf{r}_{a2}$ are position vectors to the midpoints [Eqs. (7)], i.e.,

$$\mathbf{r}_{ai} = x_{ai}\hat{\mathbf{e}}_x + h_i\hat{\mathbf{e}}_y + z_{ai}\hat{\mathbf{e}}_z \qquad (i = 1, 2). \tag{14}$$

The vectors $\hat{\mathbf{n}}'$ and $\hat{\mathbf{n}}''$ are defined in Eqs. (2). Furthermore, for $i = 1,2$,

$$\nabla h_{ai}(x, z) = h_{xai}\hat{\mathbf{e}}_x + h_{zai}\hat{\mathbf{e}}_z,$$
$$\nabla h_{ais}(x, z) = h_{xais}\hat{\mathbf{e}}_x + h_{zais}\hat{\mathbf{e}}_z. \tag{15}$$

The statistical average of σ_T over the random heights h_{ai} and slopes ∇h_{ai} is obtained on multiplying Eq. (13) by the probability density functions for the heights and the slopes at the midpoints and integrating over the heights and the slopes. Thus Eq. (13) reduces to

$$\langle \sigma_T^{PQ} \rangle \approx \frac{k_0^2}{\pi A} P_2(\hat{\mathbf{n}}^i) P_2(\hat{\mathbf{n}}^f) \sum_{P,Q=V,H} \int \left[\frac{D_{2'}^{PS}(\hat{\mathbf{n}}^f, \hat{\mathbf{n}}') D_{1'}^{SQ}(\hat{\mathbf{n}}', \hat{\mathbf{n}}') D_{2''}^{*PR}(\hat{\mathbf{n}}^f, \hat{\mathbf{n}}'') D_{1''}^{*RQ}(\hat{\mathbf{n}}'', \hat{\mathbf{n}}^i)}{(n_y^f - n_y')(n_y^f - n_y'')(n_y^i - n_y')(n_y^i - n_y'')} \right]_s$$
$$\times \exp[jk_0(\boldsymbol{\rho}_{a1} - \boldsymbol{\rho}_{a2}) \cdot (\hat{\mathbf{n}}' - \hat{\mathbf{n}}'')] \exp[-k_0^2 \langle h^2 \rangle (n_y' - n_y'')^2] p(\nabla h_{a1s}, \nabla h_{a2s}) [1 - P_2(|n_y'|)]$$
$$\times [1 - P_2(|n_y''|)] \frac{\mathrm{d}n_y' \mathrm{d}n_z' \mathrm{d}n_y'' \mathrm{d}n_z'' \mathrm{d}x_{a1} \mathrm{d}z_{a1} \mathrm{d}x_{a2} \mathrm{d}z_{a2}}{n_x' n_x'' [n_y^f - (n_y' + n_y'')/2]^2 [n_y^i - (n_y' + n_y'')/2]^2}. \tag{16a}$$

For the derivation of Eq. (16), it has been assumed that the distance between the midpoints of the pairs of points $1'$, $1''$ and $2'$, $2''$ (namely, $|\mathbf{r}_{a1} - \mathbf{r}_{a2}|$) is larger than the correlation length l_c of the surface height autocorrelation function, such that

$$\langle \exp[ik_0(n_y' - n_y'')(h_{a1} - h_{a2})] \rangle$$
$$\approx \langle \exp[ik_0(n_y' - n_y'')h_{a1}] \rangle \langle \exp[-ik_0(n_y' - n_y'')h_{a2}] \rangle$$
$$= |\chi^2[k_0(n_y' - n_y'')]|. \tag{16b}$$

When the distance between the midpoints is small compared with l_c, the elements of the four scattering matrices D^{PQ} become vanishingly small for the quasi-parallel case ($\hat{\mathbf{n}}' \approx \hat{\mathbf{n}}''$), since $[(\hat{\mathbf{n}}' + \hat{\mathbf{n}}'') \cdot \nabla h_{a1}]$, $[(\hat{\mathbf{n}}' + \hat{\mathbf{n}}'') \cdot \nabla h_{a2}] \to 0$. Furthermore, in Eq. (16), the surface element scattering coefficients D^{PQ} are evaluated at the specular points, P_2 is the shadow function,[3] and $P_2(\hat{\mathbf{n}}^i)$ and $P_2(\hat{\mathbf{n}}^f)$ are the probabilities that the rough surface is not in the shadow for the incident and scattered waves, respectively, while $[1 - P_2(|n_y|)]$ is the probability that a double-scatter event will occur. Furthermore, for $i = 1, 2$,

$$\boldsymbol{\rho}_{ai} = \mathbf{r}_{ai} - h_{ai}\mathbf{e}_\gamma \tag{17a}$$

and $p(\nabla h_{a1s}, \nabla h_{a2s})$ is the probability density function of the slopes at specular points. In Eq. (16) a Gaussian probability density function with mean square height $\langle h^2 \rangle$ has been assumed for the height of the random rough surface. To integrate with respect to the horizontal components of the midpoint position vectors, we make the following transformations:

$$\boldsymbol{\rho}_{a1} - \boldsymbol{\rho}_{a2} \equiv \boldsymbol{\rho}_{ad}, \qquad (\boldsymbol{\rho}_{a1} + \boldsymbol{\rho}_{a2})/2 \equiv \boldsymbol{\rho}_{aa}. \tag{17b}$$

The range of the integration variables x_{aa} and z_{aa} is $-l_x < x_{aa} < l_x$ and $-l_z < z_{aa} < l_z$. The integration with respect to x_{aa} and z_{aa} yields the radar footprint $A = 4l_x l_z$, since the integrand is independent of $\boldsymbol{\rho}_{aa}$. Furthermore, the integration with respect to the components of $\boldsymbol{\rho}_{ad}$ (x_{ad} and z_{ad}) yields a product of two sinc functions, since the range of the variables x_{ad} and z_{ad} is $-L_m \leqslant x_{ad} < L_m$ and $-L_m < z_{ad} < L_m$, respectively. Thus

$$\int_{-L_m}^{L_m} \int_{-L_m}^{L_m} \exp[(jk_0\boldsymbol{\rho}_{ad}) \cdot (\hat{\mathbf{n}}' - \hat{\mathbf{n}}'')] \mathrm{d}x_{ad} \mathrm{d}z_{ad}$$
$$= 2L_m \operatorname{sinc}[k_0 L_m (n_x' - n_x'')] 2L_m \operatorname{sinc}[k_0 L_m (n_z' - n_z'')], \tag{18}$$

in which L_m is the mean width of a typical depression on the rough surface.[1,4,5] The above analytical procedures reduce the 12-dimensional integral (5) (not including averaging over the random heights and slopes at two differ-

ent points on the rough surface) into a tractable four-dimensional integral over the variables n_y', n_y'', n_z', and n_z''.

Upon changing the integration variables n_y', n_y'', n_z', and n_z'' to the spherical coordinate variables θ and ϕ, one gets

$$\langle \sigma_{dp}^{PQ} \rangle = \frac{(2k_0L_m)^2}{\pi} P_2(\hat{\mathbf{n}}^i)P_2(\hat{\mathbf{n}}^f) \sum_{R,S=V,H} \int \left[\frac{[D_{2'}^{PS}(\hat{\mathbf{n}}^f, \hat{\mathbf{n}}')D_{1'}^{SQ}(\hat{\mathbf{n}}', \hat{\mathbf{n}}^i)D_{2''}^{*PR}(\hat{\mathbf{n}}^f, \hat{\mathbf{n}}'')D_{1''}^{*RQ}(\hat{\mathbf{n}}'', \hat{\mathbf{n}}^i)]}{(n_y^f - n_y')(n_y^f - n_y'')(-n_y^i + n_y')(-n_y^i + n_y'')} \right]_s$$
$$\times \frac{p(h_{xa1s}h_{xa2s}h_{za1s}h_{za2s})}{[n_y^f - (n_y' + n_y')/2]^2[-n_y^i + (n_y' + n_y'')/2]^2} [1 - P_2(|n_y'|)][1 - P_2(|n_y''|)]$$
$$\times \sin[k_0L_m(n_x' - n_z'')] \operatorname{sinc}[k_0L_m(n_z' - n_z'')] \exp[-\langle h^2 \rangle k_0^2(n_y' - n_y'')^2] \sin\theta' \sin\theta'' \, d\theta' d\theta'' d\phi' d\phi''. \quad (19)$$

It is useful to determine *a priori* the regions (defined by the four variables n_y', n_y'', n_z', and n_z'') that contribute most significantly to the like-polarized ($P = Q = V$ or H) and cross-polarized ($P \neq Q = V$ or H) bistatic double-scatter cross sections. In view of the two sinc functions and the characteristic function $\chi[k_0(n_y' - n_y'')h)]$ in the integral expression for the double-scatter cross sections [Eq. (19)], the major contribution to the integral is from the region $\hat{\mathbf{n}}' \to \hat{\mathbf{n}}''$ (quasi parallel). Furthermore, because of the shadow function $(1 - P_2)$, when these quasi-parallel paths are also quasi horizontal ($n_y' \approx 0$, $n_y'' \approx 0$), the value of the integrand in Eq. (19) peaks. To facilitate the numerical integration of relation (16), in view of the integrable singularity associated with $n_x'n_x''$ in the denominator of relation (16), the following transformations to polar coordinates are implemented for both $\hat{\mathbf{n}}'$ and $\hat{\mathbf{n}}''$:

$$n_x = \sin\theta\cos\phi, \qquad n_y = \cos\theta, \qquad n_z = \sin\theta\sin\phi,$$
$$0 < \theta < \pi, \qquad \phi_0 < \phi < 2\pi + \phi_0, \quad (20)$$

where ϕ_0 is an arbitrary constant. The product of the Jacobians of these transformations is

$$J'J'' = \sin^2\theta' \cos\phi' \sin^2\theta'' \cos\phi''. \quad (21a)$$

The ranges of the variables are $0 < \theta', \theta'' < \pi$ and $\phi_0 < \phi', \phi'' < 2\pi + \phi_0$. For the quasi-parallel case, $\phi_0 = 0$ is a suitable choice. Thus

$$dn_y'dn_y''dn_z'dn_z''/n_x'n_x'' = \sin\theta' \sin\theta'' \, d\theta' d\theta'' d\phi' d\phi''. \quad (21b)$$

Since the scattering coefficients D^{PQ} vanish for grazing incident and scatter angles, there are no singularities that are due to the product appearing below the scattering coefficients D^{PQ} in Eq. (19). For $n_y^i \to 0$, $n_y^f \to 0$ grazing incident and scatter angles, the shadow functions $P_2(\hat{\mathbf{n}}^i)$ and $P_2(\hat{\mathbf{n}}^f)$ vanish. Furthermore, when $n_y' \to 0$ and $n_y'' \to 0$, the probability for a double-scatter event $(1 - P_2) \to 1$. Thus Eq. (19) is not singular when the product appearing below the probability density function for the slopes (at the specular points) vanishes. It takes 1–2 CPU hours to evaluate the four-dimensional integrals in Eq. (19) for all four cross sections σ^{PQ} on a Silicon Graphics Computer model 4D/380VGX in the Center for Electro-Optics at the University of Nebraska-Lincoln. To make sure that the integration subroutine does not miss the very narrow region around $\theta'' \approx \theta' \approx \pi/2$ and $\phi'' \approx \phi'$, where the integrand peaks for the quasi-parallel case, and to reduce the regions of integration in Eq. (19), we subdivide the limits of integration ($0 \leq \theta', \theta'' \leq \pi$ and $0 < \phi', \phi'' \leq 2\pi$) as follows for the quasi-parallel case:

$$0 \leq \theta'' \leq \theta', \qquad \theta' \leq \theta'' \leq \pi,$$
$$0 \leq \phi'' \leq \phi', \qquad \phi' \leq \phi'' \leq 2\pi. \quad (22a)$$

It can be shown that if the medium below the rough interface [$y < h(x,z)$; μ_1, ϵ_1] is finitely conducting, the complex value of the integral $\langle \sigma_1^{PQ} \rangle$ corresponding to $0 \leq \theta'' \leq \theta'$ is equal to the complex conjugate of the value of the integral $\langle \sigma_2^{PQ} \rangle$ corresponding to $\theta' \leq \theta'' \leq \pi$. Thus it is necessary to evaluate only the real part of the integral [Eq. (19)] over half the total region of integration in Eq. (19), since

$$\langle \sigma_{dp}^{PQ} \rangle = \langle \sigma_1^{PQ} \rangle + \langle \sigma_2^{PQ} \rangle = 2 \operatorname{Re}\langle \sigma_1^{PQ} \rangle. \quad (22b)$$

As noted above, this scheme not only increases the accuracy of the numerical integration of $\langle \sigma_{dp}^{PQ} \rangle$ (since the most significant part of the integral is never missed) but also reduces the amount of computation needed to evaluate the integrals. However, no attempt has been made to parallelize the computer codes in order to decrease the computation time for parallel-processing supercomputers.

For the quasi-antiparallel double-scatter paths between points $1'$ and $2'$ and points $1''$ and $2''$ [see Fig. 1(d)], the following transformations of variables are used in Eq. (5):

$$x_{d1} = x_{s1'} - x_{s2''}, \qquad x_{d2} = x_{s2'} - x_{s1''}, \quad (23a)$$
$$z_{d1} = z_{s1'} - z_{s2''}, \qquad z_{d2} = z_{s2'} - z_{s1''}, \quad (23b)$$
$$x_{a1} = (x_{s1'} + x_{s2''})/2, \qquad x_{a2} = (x_{s2'} + x_{s1''})/2, \quad (23c)$$
$$z_{a1} = (z_{s1'} + z_{s2''})/2, \qquad z_{a2} = (z_{s2'} + z_{s1''})/2. \quad (23d)$$

Furthermore, in addition to Eqs. (9a) and (9b) (unchanged), Eqs. (9c) and (9d) are replaced by

$$h_{2''} = h_{a2} - (x_{d2}h_{xa2} + z_{dz}h_{za2})/2; \quad (24a)$$

thus

$$h_{1'} - h_{2''} = x_{d1}h_{xa1} + z_{d1}h_{za1}. \quad (24b)$$

Equations (17) (unchanged) are also used to reduce the 12-dimensional integral into a four-dimensional integral. Thus, on following the same procedures as those for the quasi-parallel case, one gets the following integral expres-

sion for the (high-frequency) quasi-antiparallel ($n'_\alpha < 0$, $n''_\alpha > 0$ or $n'_\alpha > 0$, $n''_\alpha < 0$ $_\alpha$) double-scatter cross sections:

$$\langle \sigma_{da}^{PQ} \rangle = \frac{(2k_0L_m)^2}{\pi} P_2(\hat{\mathbf{n}}^i)P_2(\hat{\mathbf{n}}^f) \sum_{R,S=V,H} \int \left[\frac{D_{2'}^{PS}(\hat{\mathbf{n}}^f, \hat{\mathbf{n}}')D_{1'}^{SQ}(\hat{\mathbf{n}}', \hat{\mathbf{n}}^i)D_{2''}^{*PR}(\hat{\mathbf{n}}^f, \hat{\mathbf{n}}'')D_{1''}^{*RQ}(\hat{\mathbf{n}}'', \hat{\mathbf{n}}^i)}{(n_y^f - n_y')(n_y^f - n_y'')(-n_y^i + n_y')(-n_y^i + n_y'')} \right]_s$$
$$\times p(h_{xa1s}, h_{xa2s}, h_{za1s}, h_{za2s}) 16/(n_y^f - n_y^i + n_y' - n_y'')\,(n_y^f - n_y^i - n_y' + n_y'')^2[1 - P_2(|n_y'|)][1 - P_2(|n_y''|)]$$
$$\times \mathrm{sinc}[k_0L_m(n_x^f + n_x^i - n_x' - n_x'')]\mathrm{sinc}[k_0L_m(n_z^f + n_z^i - n_z' - n_z'')]\exp[-\langle h^2 \rangle k_0^2(n_y^f - n_y' - n_y'' + n_y^i)^2]$$
$$\times \sin\theta' \sin\theta'' \,\mathrm{d}\theta' \mathrm{d}\theta'' \mathrm{d}\phi' \mathrm{d}\phi''. \tag{25a}$$

For the quasi-antiparallel case, the arguments of the sinc functions and the characteristic function vanish (and the integrand peaks) when $\hat{\mathbf{n}}' = -\hat{\mathbf{n}}''$ only for backscatter ($\hat{\mathbf{n}}^f = -\hat{\mathbf{n}}^i$). In Eq. (25a) the vectors $\hat{\mathbf{n}}'$ and $\hat{\mathbf{n}}''$ are expressed in terms of their polar coordinates as in Eqs. (20), except that for the quasi-antiparallel case, $\hat{\mathbf{n}}' = -\hat{\mathbf{n}}''$ ($\theta'' = \pi - \theta'$, $\phi'' = \phi' + \pi$). In relations (22a), it is convenient to choose $\phi_0 = -\pi$ for ϕ' and $\phi_0 = 0$ for ϕ'' for the quasi-antiparallel case, such that $-\pi \leqslant \phi' < \pi$ and $0 \leqslant \phi'' \leqslant 2\pi$. In this case, the limits of integration are subdivided as follows:

$$0 \leqslant \theta'' \leqslant \pi - \theta', \qquad \pi - \theta' \leqslant \theta'' \leqslant \pi,$$
$$0 \leqslant \phi'' \leqslant \phi' + \pi, \qquad \phi' + \pi \leqslant \phi'' \leqslant 2\pi. \tag{25b}$$

The slopes at the specular points for the quasi-antiparallel case are given by

$$h_{xa1s} = -(n_x^f - n_x^i + n_x' - n_x'')/(n_y^f - n_y^i + n_y' - n_y''), \tag{26a}$$
$$h_{xa2s} = -(n_x^f - n_x^i + n_x'' - n_x')/(n_y^f - n_y^i + n_y'' - n_y'), \tag{26b}$$
$$h_{za1s} = -(n_z^f - n_z^i + n_z' - n_z'')/(n_y^f - n_y^i + n_y' - n_y''), \tag{26c}$$
$$h_{xa2s} = -(n_z^f - n_z^i + n_z'' - n_z')/(n_y^f - n_y^i + n_y'' - n_y^i), \tag{26d}$$

The sharp enhancement in the backscatter direction ($-\hat{\mathbf{n}}^i = \hat{\mathbf{n}}^f$) is associated with the quasi-antiparallel ($\hat{\mathbf{n}}' \approx -\hat{\mathbf{n}}''$) double-scatter cross section [Eq. (25a)].[1,4,6,7] Note the differences in the expressions for the slopes at the specular points for the quasi-parallel and quasi-antiparallel cases (12) and (26), respectively. Equations (12) and (26) can be readily interpreted. The vectors normal to the surface at the specular points $1'$, $1''$, $2'$, and $2''$ are $\hat{\mathbf{n}}_{s1'}$, $\hat{\mathbf{n}}_{s1''}$, $\hat{\mathbf{n}}_{s2'}$, and $\hat{\mathbf{n}}_{s2''}$, respectively, where

$$\hat{\mathbf{n}}_{s1'} = \hat{\mathbf{n}}' - \hat{\mathbf{n}}^i, \qquad \hat{\mathbf{n}}_{s1''} = \hat{\mathbf{n}}'' - \hat{\mathbf{n}}^i,$$
$$\hat{\mathbf{n}}_{s2'} = \hat{\mathbf{n}}^f - \hat{\mathbf{n}}', \qquad \hat{\mathbf{n}}_{s2''} = \hat{\mathbf{n}}^f - \hat{\mathbf{n}}''. \tag{27}$$

For the quasi-parallel case $\hat{\mathbf{n}}' \approx \hat{\mathbf{n}}''$, the vectors $\hat{\mathbf{n}}_{s1'}$ and $\hat{\mathbf{n}}_{s2'}$, are also quasi parallel to the vectors $\hat{\mathbf{n}}_{s1''}$ and $\hat{\mathbf{n}}_{s2''}$, respectively, and the slopes at the midpoints between $1'$, $1''$ and $2'$, $2''$ [see Fig. 1(c)] are given by the vectors

$$\hat{\mathbf{n}}_{sap1} = (\hat{\mathbf{n}}_{s1'} + \hat{\mathbf{n}}_{s1''})/2, \quad \hat{\mathbf{n}}_{sap2} = (\hat{\mathbf{n}}_{s2'} + \hat{\mathbf{n}}_{s2''})/2, \tag{28}$$

corresponding to the slopes in Eqs. (12). Similarly, for the antiparallel case $\hat{\mathbf{n}}' \approx -\hat{\mathbf{n}}''$, the slopes at the midpoints between $1'$, $2''$ and $1''$, $2'$ [see Fig. 1(d)] are given by the components of the vectors

$$\hat{\mathbf{n}}_{saa1} = (\hat{\mathbf{n}}_{s1'} + \hat{\mathbf{n}}_{s2''})/2, \qquad \hat{\mathbf{n}}_{saa2} = (\hat{\mathbf{n}}_{s1''} + \hat{\mathbf{n}}_{s2'})/2, \tag{29}$$

corresponding to the slopes in Eqs. (26). Furthermore, the integrand in Eq. (19) peaks when the pairs of vectors $\hat{\mathbf{n}}_{s1'}$, $\hat{\mathbf{n}}_{s1''}$ and $\hat{\mathbf{n}}_{s2'}$, $\hat{\mathbf{n}}_{s2''}$ are parallel to each other, namely,

$$\hat{\mathbf{n}}_{sdp} = \hat{\mathbf{n}}_{s1'} - \hat{\mathbf{n}}_{s1''} = \hat{\mathbf{n}}_{s2'} - \hat{\mathbf{n}}_{s2''} = \hat{\mathbf{n}}' - \hat{\mathbf{n}}'' = 0. \tag{30}$$

The integrand in Eq. (25a) peaks when the pairs of vectors $\hat{\mathbf{n}}_{s1'}$, $\hat{\mathbf{n}}_{s2''}$, and $\hat{\mathbf{n}}_{s1''}$, $\hat{\mathbf{n}}_{s2'}$, are parallel, namely,

$$\hat{\mathbf{n}}_{sda} = \hat{\mathbf{n}}_{s1'} - \hat{\mathbf{n}}_{s2''} = \hat{\mathbf{n}}_{s1''} - \hat{\mathbf{n}}_{s2'}$$
$$= \hat{\mathbf{n}}' + \hat{\mathbf{n}}'' - \hat{\mathbf{n}}^f - \hat{\mathbf{n}}^i \to 0. \tag{31}$$

Note that for Eq. (30) to be satisfied, the paths must be parallel; however, for Eq. (31) to be satisfied, the paths must be antiparallel for backscatter only. This distinction between the quasi-parallel case and the quasi-antiparallel case explains why the enhanced backscatter is associated only with the quasi-antiparallel case.

For backscatter at normal incidence, the major contributions to the double-scatter cross sections are associated with the quasi-horizontal paths between points 1 and 2 [see Fig. 1(d)], and the slopes at the stationary points are approximately $\pm 45°$. The integrands in the final expressions for the double-scatter cross sections [Eqs. (19) and (25)] peak for a very small range of angles at which $\hat{\mathbf{n}}'$ and $\hat{\mathbf{n}}''$ are quasi horizontal ($n_y' \approx 0$ and $n_y'' \approx 0$), as a result of the presence of $1 - P_2$ in the integrand. The characteristic functions

$$\chi[k_0(n_y' - n_y'')] = \exp[-\langle h^2 \rangle k_0^2(n_y' - n_y'')^2/2],$$
$$\chi[k_0(n_y^f + n_y^i - n_y' - n_y'')]$$
$$= \exp[-\langle h^2 \rangle k_0^2(n_y^f + n_y^i - n_y' - n_y'')^2/2]$$

in Eqs. (19) and (25) peak for $(n_y' - n_y'') \to 0$ (quasi parallel) and $(n_y^f + n_y^i - n_y' - n_y'') \to 0$ (quasi antiparallel and backscatter), respectively. For the illustrative examples, Eqs. (19) and (25) are used to evaluate the bistatic double-scatter cross sections. The corresponding high-frequency single-scatter cross sections are

$$\langle \sigma_s^{PQ} \rangle = 4\pi |D^{PQ}(\hat{\mathbf{n}}^f, \hat{\mathbf{n}}^i)|^2 p(h_{xs}, h_{zs})/(n_y^f - n_y^i)^4,$$
$$P = Q, \qquad \langle \sigma_s^{PQ} \rangle = 0, \qquad P \neq Q, \tag{32}$$

since the incident waves are not depolarized at the specular points in the plane of incidence.

3. ILLUSTRATIVE EXAMPLES

The incoherent single- and double-scatter cross sections (quasi parallel+quasi antiparallel), as well as the total (single+double) cross sections, for two-dimensional rough surfaces are plotted in Figs. 2–10 as functions of the scatter angles $\theta^f \cos\phi^f$ (where $\phi^f = 0,\ \pi$). The two-dimensional rough surface is assumed to be coated with gold permittivity $\epsilon_r = -9.888312 - j1.051766$ at $\lambda = 0.633\,\mu$m. The incident angles are $\theta^i = 10°$, $\phi^i = 0$. The Rayleigh roughness parameter is $\beta = 4k_0^2\langle h^2\rangle$. In Figs. 2–4, the single-scatter cross sections are plotted as functions of the scatter angles $\theta^f \cos\phi^f$, $\phi^f = 0$ and π. In Fig. 2 the polarizations of the incident and scattered waves are vertical (parallel). The Rayleigh roughness parameter $\beta = 4k_0^2\langle h^2\rangle$ varies from 10 to 394, and the mean square slope is mss = 0.5. The single-scatter incoherent cross sections are insensitive to $\langle h^2\rangle$, since, for the entire range of the parameters considered, $\beta \gg 1$. They are sensitive to $\langle h^2\rangle$ when $\beta < 1$. They are proportional to $\langle h^2\rangle$ for $\beta \ll 1$ where the coherent scatter cross sections are not small. For $\beta \gg 1$ the coherent cross sections are negligible.

In Fig. 3 the polarizations of the incident and scattered waves are vertical (parallel), and the mss varies from 0.25 to 1.0 and $\beta = 394$. For the range of parameters considered, the single-scatter cross sections decrease as the mss increases, while the double-scatter cross sections increase with increasing mss. As the mss becomes larger than unity, the values of both the single- and double-scatter cross sections saturate.

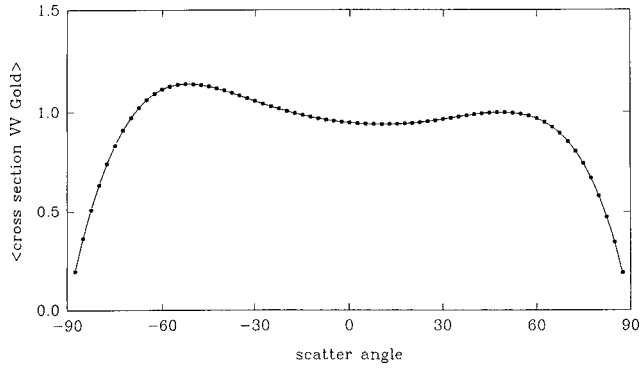

Fig. 2. Single-scatter vertical-to-vertical radar cross section. Mean square height (Rayleigh parameter β) is the variable parameter $110 \leqslant \beta \leqslant 394$. The mean square slope (mss) value is 0.5. The following parameters apply to Figs. 2–10: incident angle of 10°, relations permittivity of $-9.888312/j1.051766$, and wavelength of 0.633 μm.

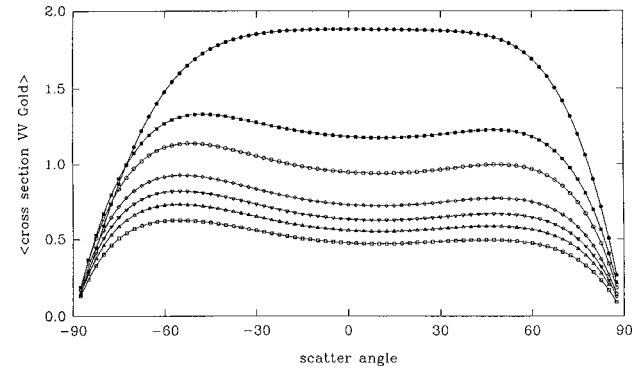

Fig. 3. Single-scatter vertical-to-vertical radar cross section. Mean square slope (mss) is the variable parameter, and the curves from top to bottom correspond to mss values of 0.25, 0.4, 0.5, 0.65, 0.75, 0.85, and 1.0. The value of β is 394.

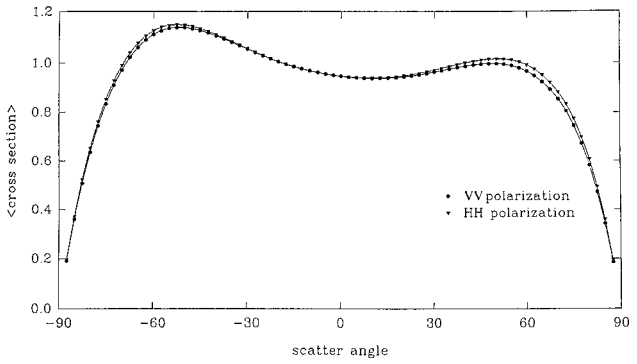

Fig. 4. Single-scatter like-polarized radar cross section for vertical to vertical (lower curve) and horizontal-to-horizontal (upper curve) polarization. The mss and β values are 0.5 and 394, respectively.

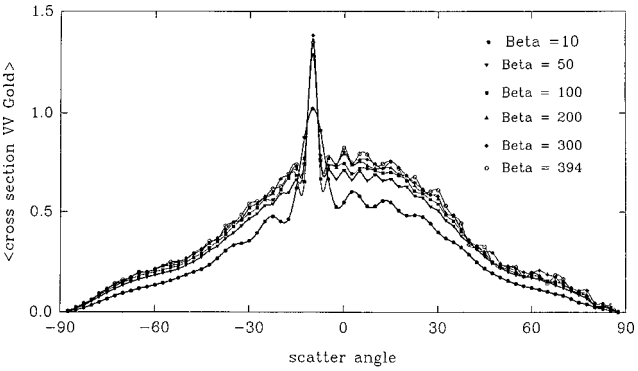

Fig. 5. Double-scatter radar cross section. Mean square height (Rayleigh parameter β) is the variable parameter (quasi-parallel and quasi-antiparallel contributions added). The polarization is vertical to vertical. The mss value is 0.5. Lowest curve, $\beta = 10$. Data saturate as β increases.

In Fig. 4 the single-scatter cross sections are plotted for both vertical (parallel) and horizontal (perpendicular) polarizations. The results indicate that for the given values of $\beta = 394$ and mss = 0.5, the single-scatter cross sections are practically the same for both like polarizations.

In Figs. 5–7 the double-scatter cross sections are plotted as functions of the scatter angles $\theta^f \cos\phi^f$, $\phi^f = 0$ or π. These three illustrations correspond to the cases considered in Figs. 2–4.

In Fig. 5 the polarizations of the incident and scatter waves are vertical (parallel). The roughness parameter β increases from 10 to 394, and mss = 0.5. The double-scatter cross sections (unlike the single-scatter cross sections) are sensitive to variations in β. The cross sections increase as β increases, and they practically merge for $\beta > 100$. For $\beta \gg 100$ higher-order multiple-scatter cross section are not negligible.

In Fig. 6 the polarizations of the incident and scattered waves are vertical (parallel). The roughness parameter $\beta = 394$, and the mss varies from 0.25 to 1. Both β and the mss are dimensionless quantities, since the slope is

dimensionless and $k_0 = 2\pi/\lambda$ is measured in units of inverse meters. The double-scatter cross sections are more sensitive to variations in mss than to those in β. Unlike the single-scatter cross sections, the double-scatter cross sections increase rather than decrease as mss increases, and they begin to merge for mss > 0.75. The level of the enhanced backscatter increases as both the roughness parameter β and mss increase. However, they merge for $\beta > 100$ and mss > 0.75. The angular width of the backscatter cross sections decreases as β increases; however, the angular width is practically insensitive to variations in the mss for the range of parameters considered.

In Fig. 7 all four like- and cross-polarized double-scatter cross sections are plotted as functions of the scatter angles $\theta^f \cos\phi^f$, $\phi^f = 0$. The level and the angular width of the backscatter enhancement for all four cross sections are practically the same, except that the values of the cross-polarized cross sections decrease somewhat faster as $\theta^f \to 90°$ (grazing angles). For the illustrative examples, the first and second letters ($P = V, H$; $Q = V, H$) correspond to the polarizations of the scattered and incident waves, respectively.

In Figs. 8–10, the total (single+double) scatter cross sections are plotted as functions of the scatter angles. These three illustrations correspond to the cases considered in Figs. 2–4 and 5–7. In Fig. 8 the total cross section, for the vertically polarized case, is plotted with β as the variable parameter, from $\beta = 10$ to $\beta = 394$, while mss $= 0.5$. The total scatter cross sections increase as β increases, and the results merge for $\beta > 50$. The angular width of the enhancement decreases as β increases. As noted above, the results saturate for $\beta \gg 1$.

In Fig. 9 the total cross sections for the vertically polarized case are plotted as functions of the scatter angles, with mss as the variable parameter, from mss $= 0.25$ to

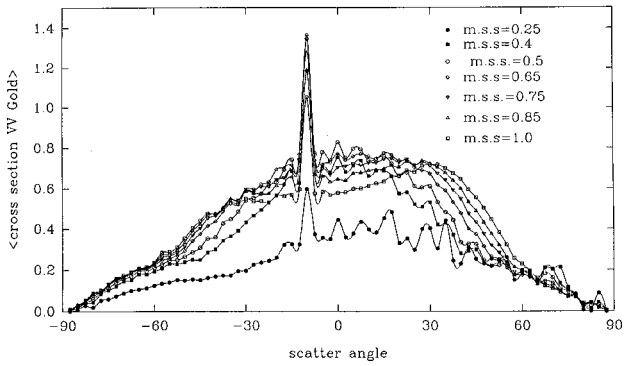

Fig. 6. Double-scatter radar cross section. The variable parameter is the mss (quasi-parallel and quasi-antiparallel contributions added). The polarization is vertical to vertical. The value of β is 394. Lowest curve, mss $= 0.25$. Data saturate as mss increases.

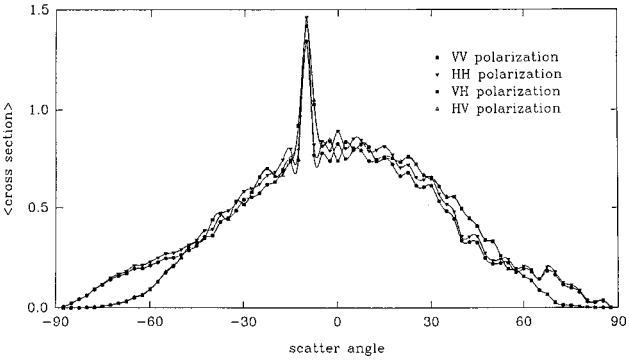

Fig. 7. Double-scatter radar cross sections for both like-polarized and both cross-polarized cases (quasi-parallel and quasi-antiparallel contributions added). The mss and β values are 0.5 and 394.105, respectively. Cross-polarized data are lower near grazing angles.

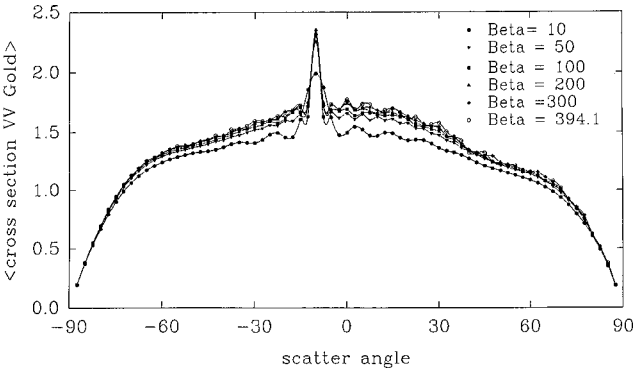

Fig. 8. Single- and double-scatter radar cross sections added. The variable parameter is β. The polarization is vertical to vertical. The mss value is 0.5. Lowest curve, $\beta = 10$. Data saturate as β increases.

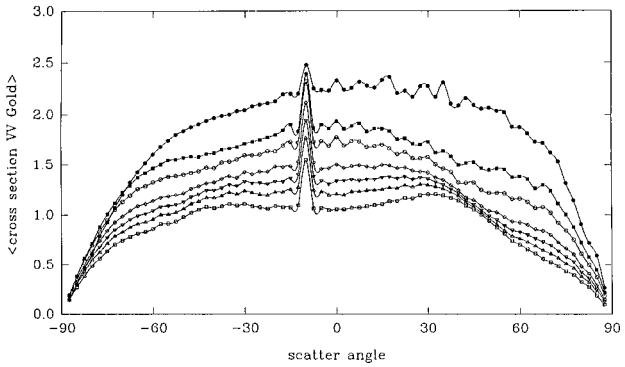

Fig. 9. Single- and double-scatter radar cross sections added. The variable parameter is the mss, and the curves from top to bottom correspond to mss values of 0.25, 0.4, 0.5, 0.65, 0.75, 0.85, and 1.0. The value of β is 394. The polarization is vertical to vertical.

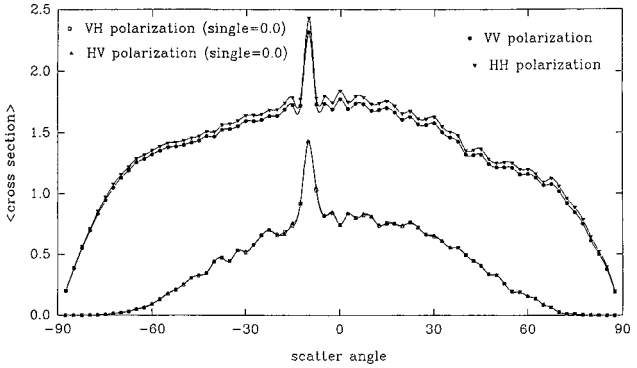

Fig. 10. Single- and double-scatter radar cross sections added for both like-polarized and both cross-polarized cases. The mss and β values are 0.5 and 394, respectively. Upper curves, HH followed by VV. Lowest curves, VH and HV merge.

mss = 1.0. For the cases considered, the total cross sections decrease as the mss increases because the contributions of the single-scatter cross sections dominate the results. The level of the backscatter enhancement increases as mss increases. However, the angular width of the enhancement does not vary significantly with changing mss. Also, as noted above, the results saturate for mss greater than unity.

In the last illustration, Fig. 10, the total scatter cross sections are plotted for all four (like and cross) polarizations. The fixed parameters are $\beta = 394$ and mss = 0.5. The like-polarized cross sections (*VV* and *HH*) are significantly larger than the corresponding cross-polarized cross sections (*VH* and *HV*). This is because the stationary-phase (high-frequency) approximations for the cross-polarized, single-scatter cross sections are negligible for scatter angles in the plane of incidence.[1,4,5] At the specular points in the plane of incidence ($\phi^f = 0, \pi$), the scattered waves are not depolarized.[8] For scattering out of the incident plane, the scattered waves do depolarize. This results in nonvanishing cross-polarized, double-scatter cross sections, even in the plane of incidence.[9] There are two mechanism's for the generation of the cross-polarized, double-scatter cross sections. Schematically, these are given by

$$V \to V \to H, \qquad V \to H \to H,$$

$$H \to H \to V, \qquad H \to V \to V.$$

In the above the first letter corresponds to the polarization of the incident wave, the second is the polarization of the single-scatter wave, and the third is the polarization of the double-scatter wave.

4. CONCLUSIONS

The results for the double-scatter radar cross sections exhibit sharp enhancements in the backscatter direction at normal and oblique incident angles. This sharp enhancement is associated with the quasi-antiparallel double-scatter path. The height and the width of the peak in the backscatter direction depend on the mean square height and slope of the two-dimensional random rough surface. The high-frequency approximations make the computations numerically tractable; however, the polarization dependence of the cross section is less obvious.[1,4]

ACKNOWLEDGMENTS

This work was supported partially by the Department of Electrical Engineering and the Center for Electro-Optics at the University of Nebraska-Lincoln and the Supercomputer facility at Cornell University. The manuscript was prepared by M. Jane Craig.

Address correspondence to Ezekiel Bahar at the location on the title page or by e-mail, bahar@dragon.unl.edu.

REFERENCES AND NOTES

1. E. Bahar and M. El-Shenawee, "Enhanced backscatter from one dimensional random rough surfaces—stationary phase approximations to full wave solutions," J. Opt. Soc. Am. A **12**, 151–161 (1995).
2. E. Bahar and Y. Zhang, "A new unified full wave approach to evaluate the scatter cross sections of composite random rough surfaces," IEEE Trans. Geosci. Remote Sens. **34**, 973–980 (1996).
3. M. I. Sancer, "Shadow-corrected electromagnetics scattering from a randomly rough surface," IEEE Trans. Antennas Propag. **AP-17**, 577–585 (1969).
4. E. Bahar and M. El-Shenawee, "Vertically and horizontally polarized diffuse double scatter cross sections of one dimensional random rough surfaces that exhibit enhanced backscatter—full wave solutions," J. Opt. Soc. Am. A **11**, 2271–2285 (1994). An extensive list of references on backscatter enhancement is published here.
5. M. El-Shenawee and E. Bahar, "Double scatter cross sections for two dimensional random rough surfaces—high frequency approximation," presented at the 1995 IEEE AP-S International Symposium and UNC/URSI Radio Meeting, Newport Beach, Calif., June 18–23, 1995.
6. A. A. Maradudin and E. R. Méndez, "Enhanced backscattering of light from weakly rough, random metal surfaces," Appl. Opt. **32**, 3335–3343 (1993).
7. A. Ishimaru and J. S. Chen, "Scattering from very rough surfaces based on the modified second order Kirchhoff approximation with angular and propagation shadowing," J. Acoust. Soc. Am. **88**, 1877–1883 (1990).
8. E. Bahar, E. M. Herzinger, and M. A. Fitzwater, "Incoherent like and cross polarized cross sections of an anisotropic rough sea surface with swell," J. Geophys. Res. [Oceans] **94**, 2159–2169 (1989).
9. M. El-Shenawee and E. Bahar, "Double scatter radar cross sections for two dimensional random rough surfaces that exhibit backscatter enhancement," presented at the meeting of the Applied Computational Electromagnetic Society, Monterey, Calif., March 18–22, 1996.